EMoD: Efficient Motion Detection of Device-free Objects Using Passive RFID Tags

Kun Zhao*, Chen Qian§, Wei Xi*, Jisong Han*, Xue Liu†, Zhiping Jiang*, Jizhong Zhao*
Xi'an Jiaotong University*
University of Kentucky§
McGill University†

***Abstract*—Efficient and accurate tracking of device-free objects is critical for anti-intrusion systems. Prior solutions for device-free object tracking are mainly based on costly sensing infrastructures, resulting in barriers to practical applications. In this paper, we propose an accurate and efficient motion detection system, named EMoD, to track device-free objects based on cheap passive RFID tags. EMoD is the first RFID system that can estimate the moving direction as well as the current location of a device-free object by measuring critical power variation sequences of passive tags. Compared with previous solutions, the unique advantage of EMoD, *i.e.*, the capability to estimate moving directions, enables object tracking using a much sparser tag deployment. We contribute to both theory and practice of this phenomenon by presenting the interference model that precisely explains it and using extensive experiments to validate it. We design a practical EMoD based intrusion detection system and implement a prototype by commercial off-the-shelf (COTS) RFID reader and tags. The real-world experiments results show that EMoD is effective in tracking the trajectory of moving object various environments.**

***Keywords*-Device-free; Motion detection; Critical state;**

I. Introduction

Wireless sensing systems have been serving as a core component of critical infrastructures and industrial control systems recently. Typically, they are built upon sensors and control units for control and protection of a physical infrastructure. Real-time sensing plays an important role in combining the computational and physical worlds together for these industrial applications.

One of the fundamental tasks of a wireless sensing system is to detect and track intruders to ensure the safety of lives and properties. Since intruders are uncooperative objects, they are impossible to be bound with specific devices. Therefore detection of device-free intruders is a core requirement of an automatic anti-intrusion system. Specific sensing devices, such as the passive infrared (PIR) sensors, sonic sensors, and video camera sensors have been used for device-free motion detection and tracking. However, these solutions incur significant cost concerns.

Recently, Radio Frequency IDentification (RFID) has become a promising technique for device-free intrusion detection. An RFID reader may observe and analyze signal changes of pre-deployed tags to infer the motion of an intruder. RFID-based motion detection is an attractive solution due to the convenient and cost-efficient deployment of RFID tags in physical environments. In fact, RFID tags have been widely applied to identification and monitoring tasks in industrial control systems for applications already, including logistics, inventory, and retailing. Reusing the existing RFID infrastructure further saves the cost of a real-time motion detection system.

However, existing RFID-based motion detection methods in the literature [1], [2], [3] are mostly based on active tags, which are less ubiquitous and much more expensive than passive tags. Existing passive tag based motion detection methods are device-based and not suitable for intrusion detection [4], [5], [6]. Meanwhile, many of them require customized devices [7], [8], [9], [10] or specialized signals [11], [15]. To the best of our knowledge, the most recent device-free object tracking system using passive tags is Twins [16]. The idea of Twins are derived from the following observation. The mutual interference between two physical immediate readable tags caused by coupling effect will make one or both of them unreadable, which is called the *critical state*. The two coupled tags are named twins[1]. If one object moves around the twins, it will cause extra RF wave reflection to the tags such that unreadable tags may accumulate sufficient power, and thus be able to backscatter their responses. In this way, the Twins system can report a nearby motion via the state shift from unreadable to readable.

In this work, we present an accurate and Efficient Motion Detection System for device-free objects using an infrastructure constructed by passive tags, named EMoD. EMoD significantly improves Twins in the two following aspects. First, Twins can only tell the location of an object but does not provide the moving direction. *EMoD is first method to report both location and direction information of a device-free object with passive RFID tags*. With the direction information, the accuracy of inferred moving trajectory can be significantly improved. More specifically, since EMoD can infer trajectory through direction information, EMoD can draw the complete trajectory employing much fewer devices (including readers and antennas) than Twins', which can dramatically reduce the deployment overheads. Second, the Twins system depends on a grid of passive tag pairs (twins) that fully cover the area of interest to localize device-free objects. In practice, the layout

[1]We use "Twins" to refer to the overall motion detection system in [16] and "twins" to refer to the specific tag pair used in Twins.

of inventory or warehouse areas is usually arranged as several pick aisles that have racks on both sides. Perpendicular to the pick aisles, several cross aisles separate the area, as shown in Fig. 1. In this typical layout, EMoD only requires a few twins pairs deployed at the *critical points*, including the entrance, exit, and intersections. Such deployment is much sparser than the requirement of the original Twins system. Therefore, the communication collision between tags and reader can be instantly relieved.

Our contribution are summarized as follows.

- We are the first to achieve direction indication of device-free objects using passive RFID tags. EMoD is built upon both the observations from experiments and theoretical modeling of backscatter communication. To the best of our knowledge, there is no prior solution in the literature that can achieve motion detection of device-free objects with a sparse deployment of passive tags.
- Based on the device-free motion detection method using passive RFID tags, EMoD can accurately and efficiently track the trajectory of moving object without taking any extra device. Comparing the existing methods such as Twins, the most advantage of EMoD, *i.e.*, the capability to estimate moving directions, enables EMoD to achieve higher tracking accuracy with fewer tags and readers.
- We have implemented the EMoD system using COTS RFID devices. According to our real world experiments, EMoD has high detection accuracy of moving direction, and the average accuracy is more than 90%.

The rest of paper is organized as follows. In Section II, we present the related work. In Section III, we describe the fundamentals of direction indication of moving objects. In Section IV, we present the design of the EMoD system. In Section V, we discuss some related topics of the proposed system. We show the experimental results in Section VI and conclude this work in Section VII.

II. Related Work

Tracking device-free moving objects, such as intruders, is a big challenge for wireless control and monitoring systems. The current approaches usually actively track the stolen properties or passively detect the moving object by deploying surveillance devices in the area of interest. Existing solutions can be categorized into device-based and device-free approaches.

Device-based approaches. Most RFID tracking methods require binding objects or persons with tags [4], [5], [6], [15], [17], [18], [19]. Although device-based solutions can achieve high localization accuracy (sub-centimeter level [15]), attaching a tag to a moving object or person is infeasible for anti-intrusion applications.

Device-free approaches. Device-free approaches are more suitable for localizing and tracking uncooperative targets [1], [9], [12], [13], [14], [21], [22], [23]. The basic idea is to detect the signal changes of pre-deployed tags caused by the moving objects. Most existing works rely on active RFID tags. LANDMARC [1] is a pioneer work which uses active RFID tag array to cover the area of interest. The position of a target is determined by comparing the RSS reported by the deployed tags to the fingerprint database constructed in advance. [2] and [24] are two improvement works that also use an active tag grid to achieve advanced device-free human trajectories tracking and classification. AutoWitness [25] is a property-tracking system based on a customized tracking device. Such a tracker can log the readings of its motion sensors and the IDs of nearby cellular towers. Once having detected available network access, the tracker sends the logged records to the tracking center. Its trajectory is thereby recovered using a Viterbi Decoding algorithm. The tracking delay of AutoWitness is about 5 minutes, which does not satisfy many application requirements. PassiveLoc [26] is another active RFID based indoor localization system. It monitors the RSS variance caused by human movements. A person's position could be estimated by fingerprinting the monitoring field. One of its following works, SCPL [27], achieves human tracking based on radio linking quality.

For active tag based systems, the concerns of device and deployment cost form the largest barrier to real large-scale systems. Therefore, researchers have started the investigation of passive tag based solutions. TASA [3] employs both the active and passive tags in a device-free localization system, in which the active tags serve to improve the localization accuracy in the hybrid RFID tag array. The most recent and relevant work is Twins [16]. As aforementioned, the Twins system leverages a deliberately generated state between two adjacent tags to detect nearby moving objects. Different from Twins, EMoD is a new motion detection system using sparse deployment of tags to achieve real-time and accuracy requirements.

Besides RFID tags, other devices are also utilized for device-free motion detection and object tracking. By synchronizing the camera network with a wireless sensor network, TelosCam[28] enables the surveillance camera to "see" the stolen properties behind the wall. Tracking human or objects based on Wi-Fi is intuitive, for Wi-Fi signals are ubiquitous. Omni-PHD [29] provides a Channel State Information (CSI) based omni-directional human detection leveraging the multi-path effect. Pilot [30] is a device-free system to locate individual target. However, it requires a dense site-survey. FCC [31] presents a device-free human crowd estimation system with little training overhead. The popularity of Software Defined Radio (SDR) empowers the researches on passive sensing. Wi-Vi [7] and WiTrack [8] enable passive motion sensing in the through-the-wall and 3D modes, respectively. Gesture recognition is achieved by Wi-See [9] while Wi-Track2.0 [11] can accomplish multi-person localization. However, the expensive hardware and relatively short sensing range still prohibit SDR-based approaches from practical use.

III. Fundamentals of Direction Indication

The main challenge (and contribution) of our passive RFID based system is to accurately predict the direction of a moving

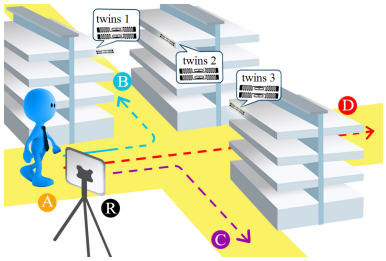

Fig. 1. Deployment scenario

object in real-time. Addressing this issue significantly reduces the deployment cost and increases detection efficiency.

The fundamentals of the proposed direction indication algorithm is based upon both the observations from experiments and theoretical modeling of backscatter communication. We summarize our findings as follows.

- We define the *critical power* (CP) of a tag as the power of the transmission (reader) with which the tag can be turned into its critical state. For per-location of an intruder, monotonic relationship between the CP of deployed tags and the position of the object does not hold.
- However, for whole-trajectory in each monitoring intersection, a unique correspondence between the features of CP sequence and trajectory holds well, *i.e.*, the distribution of the CP matrix can be used as an indicator for plotting an intruder's trajectory.

In the following subsections, we detail the theoretical analysis supporting the above claims, and present the verification result of indoor experiments.

A. Impact of object location to received power

Utilizing the electric field intensity, we establish the functional relationship between the average power density and the object's location.

A tag's average power density is determined by the electric field intensity. According to the Poynting theorem [32], the time-average power density $\langle S \rangle$ at position z can be calculated as:

$$\langle S \rangle = \frac{1}{2\eta} E_z^2 \tag{1}$$

where E_z is the norm of electric filed intensity at z, and $\eta = \sqrt{\frac{\mu}{\varepsilon}} \approx 120\pi\Omega$ is the intrinsic impedance of free space. Furthermore, the electric filed intensity is determined by the location of moving object's in a stationary environment.

The wireless channel between the transmitter antenna and receiver antenna can be modeled as a linear time-varying (LTV) system [32]. In a stationary environment, *i.e.*, the antenna and tags are fixed, the electric intensity can be separated into two parts: the stable environmental effect and the moving object's effect. We describe the stable (non-person) scenario at first, and then superimpose the moving object's influence.

1) Environmental effect: Assuming the reader's transmit intensity is $\mathbf{E_R}$, the received intensity of the tag in a stable scenario $\mathbf{E_T^S}$ can be denoted as

$$\mathbf{E_T^S} = \mathbf{E_R} \sum_{i=0}^{m} \Gamma_i L_{RT_i} \cos(\omega t - \varphi_i)$$

where m, Γ_i, L_{RT_i}, φ_i are the number of distinguishable paths, the reflections of obstacles' surface along the ith path, the path loss of the ith path from the reader to the tag, and the corresponding phase delay, respectively.

According to the phasor formula [33], we have

$$\mathbf{E_T^S} = \mathbf{E_R} \mathfrak{A}_{RT} \cos(\omega t - \varphi_{RT}) \tag{2}$$

and

$$\begin{cases} \mathfrak{A}_{RT} = \left(\sum_{i=0}^{m} \Gamma_i L_{RT_i} \cos\varphi_i \right)^2 + \left(\sum_{i=0}^{m} \Gamma_i L_{RT_i} \sin\varphi_i \right)^2 \\ \varphi_{RT} = \arctan \dfrac{\sum_{i=0}^{m} \Gamma_i L_{RT_i} \sin\varphi_i}{\sum_{i=0}^{m} \Gamma_i L_{RT_i} \cos\varphi_i} \end{cases}$$

where $\mathfrak{A}_{RT}$ and φ_{RT} denote the path loss and phase delay contributed by all multipath components, respectively.

2) Moving object effect: When an object P enters into this area, it changes the electromagnetic field distribution. The intensity contributed by the moving object [32] is

$$\mathbf{E_T^P} = \mathbf{E_R} \mathfrak{A}_P \cos(\omega t - \varphi_P)$$

where $\mathfrak{A}_P$ and φ_P denote the path loss and phase delay contributed by the intrusive object.

Due to the linearity of LTV, the joint intensity $\mathbf{E_T}$ can be calculated as

$$\begin{aligned} \mathbf{E_T} &= \mathbf{E_T^S} + \mathbf{E_T^P} \\ &= \mathbf{E_R}(\mathfrak{A}_{RT} \cos(\omega t - \varphi_{RT}) + \mathfrak{A}_P \cos(\omega t - \varphi_P)) \end{aligned} \tag{3}$$

Using the phasor formula again and substituting (3) into (1), we have

$$\begin{aligned} \langle S \rangle &= \frac{1}{2\eta} E_T^2 \\ &= \frac{1}{2\eta} E_R^2 \big(\mathfrak{A}_P^2 + 2\mathfrak{A}_P \mathfrak{A}_{RT} \\ &\quad \cdot \cos(\varphi_P - \varphi_{RT}) + \mathfrak{A}_{RT}^2 \big) \end{aligned} \tag{4}$$

Assuming the coordinates of the reader, tag and object are $R = (X_R, Y_R)$, $T = (X_T, Y_T)$ and $P = (X_P, Y_P)$, respectively, the length of trajectory $\overline{RPT}$ from the reader to the tag via the object is $d_{RPT} = \sqrt{(X_P - X_R)^2 + (Y_P - Y_R)^2} + \sqrt{(X_T - X_P)^2 + (Y_T - Y_P)^2}$.

The path loss on $\overline{PRT}$ can be modeled as

$$\mathfrak{A}_P = \frac{\alpha \Gamma_P}{d_{RPT}} \tag{5}$$

where α is a proportionality constant [33]. Due to the half-wave loss phenomenon [32], the equivalent phase delay is

$$\varphi_P = 2\pi \frac{d_{RPT}}{\lambda} - \pi \tag{6}$$

Therefore, we can see that the average power density of tag $\langle S \rangle$ is determined by the transmitting power density $\frac{E_R^2}{2\eta}$, environmental parameters $\mathfrak{A}_{RT}$ and φ_{RT}, and the location based parameters $\mathfrak{A}_P$ and φ_P. The last two parameters are correlated with the moving object's position, as shown in (5) and (6). In other words, if the environment remains unchanged, the received power of the tag is only determined by the object's location, *i.e.*,

$$\langle S \rangle = f(\mathfrak{A}_P, \varphi_P) = f(P)$$

It is worth to note that a power density $\langle S \rangle$ is not one-to-one correlated to a unique location P, due to the non-monotonic relationship shown in (4). Thus, we are aiming to extract a power sequence uniquely mapping to the moving target's trajectory.

B. Weak correlation between trajectory and power sequence

Denote the moving target's trajectory and the corresponding power sequence as $T = \langle t_1, t_2, \cdots, t_m \rangle$ and $S = \langle s_1, s_2, \cdots, s_m \rangle = \langle f(t_1), f(t_2), \cdots, f(t_m) \rangle$, respectively. Theoretically, same trajectories should have same power sequences. Due to the fading and noise, the measured power sequences, however, are not always the same, when the object moves along the same trajectory. There are two main reasons incurring this phenomenon:

1) Training samples cannot exactly follow the same position t_i of the trajectory, so there is an error at each trajectory position. We name such an error as a position based error (PBE), and exploit the discretization and morphological opening operation to solve this problem.
2) When an intruder enters an area under surveillance, the first trajectory position might be t_2 or t_3, but not t_1. In other words, the trajectory sequences are mismatched, and need to be aligned. We name this kind of errors as the initial bias (IB), and exploit the morphological dilation to solve this problem.

These two problems make it difficult to directly estimate the trajectory according to the power sequence. We solve them using the mathematical morphology, which will be detailed in Section IV.

C. Experimental validation for theoretic analysis

We conduct indoor experiments to verify the properties derived from the theoretical analysis. Fig. 2 shows an example of CP sequences with different trajectories. There are three twins deployed in the intersection as shown in Fig. 1. The colored map denotes the time sequence from the first sample to 200^{th} sample. Three axes denote the CP values of three twins. Subfigures (a) and (d) with circles show the CP distributions of two turning-left experiments. Subfigure (b) with lower-triangular shows the CP distribution of going-straight while subfigure (c) with upper-triangular shows the results of turning-right, respectively. Obviously, different trajectories have different CP distributions, while the same trajectories have similar CP distributions with some inconsistent values.

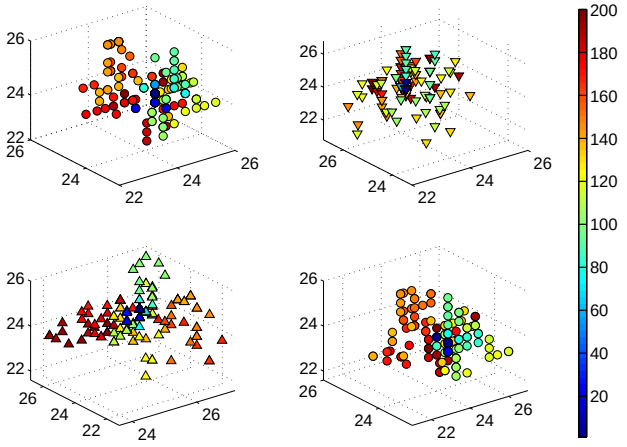

Fig. 2. CP variance with different moving trajectories

Hence, collecting such sequences and extracting their features is possible to identify the motion direction of objects. This heuristic correlation has not been disclosed by prior works, because they merely provide a "0/1" judgment to indicate whether the object is detected or not, resulting in a degradation in both the accuracy and efficiency.

IV. System Design

Based on the theoretical analysis and experimental results presented in Section III, we propose a device-free method to recognize and predict an intruder's movement direction. As shown in Fig. 3, our algorithm consists of three phases, 1) data preprocessing, 2) motion profile extraction, and 3) trajectory recognition.

A. Data preprocessing

The data preprocessing phase achieves three functions: PBE elimination, intrusion detection, and sequence normalization.

1) PBE Elimination: As stated in Section III-B, in the PBE elimination step, we need to remove the impacts of PBE. If the object moves along the same trajectory, the variance of power sequence caused by PBE is $\Delta s_i \approx \Delta t_i \frac{df}{dt} \mid_{t=t_i}$. It can be deduced by casting the 1^{st} order Taylor formula to (4). Since Δt_i is much less than the length of the trajectory, Δs_i is much less than the power variation. Therefore, by setting reasonable threshold parameters, we can discretize the power into a trichotomous number c (*i.e.*, $1, 0, -1$), which represents the increase, stableness, and decrease of the tag's CP, respectively. As mentioned in Section III, objects at different locations will have different effects on the tag's CP. In some locations, the object reflects RF signals, which will inject more RF waves to the tag such that it can be read with a smaller CP, where $c = 1$. In some locations, the object blocks the transmission from the reader to tag, weakening the power received by the tag such that it should be read with a larger CP, where $c = -1$. In the other locations, the object has little impact on the tag's CP, where $c = 0$.

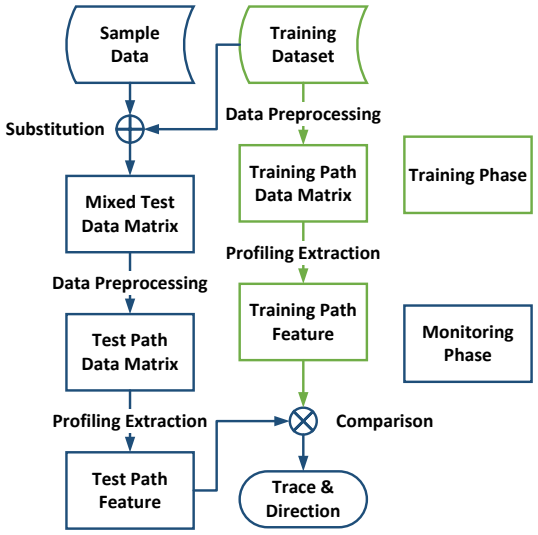

Fig. 3. Workflow of EMoD

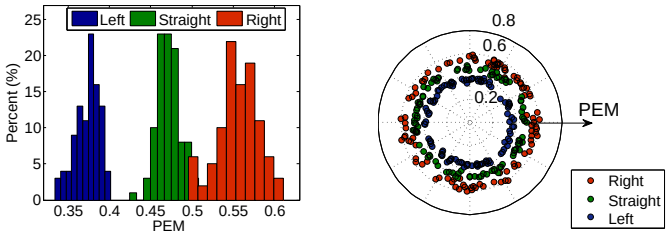

Fig. 4. PEM values of three directions can be clearly clustered.

2) Intrusion Detection: The reader continuously scans the CP of each tag and obtains a sequence of its trinary c. In order to react to intrusions efficiently, the reader should filter abundant runs of "0"s out, because there is no intrusion in those runs. Note that we only filter outer "0"s but not inner "0"s which are between "1"s or "-1"s.

3) Sequence Normalization: Additionally, the length of trinary sequence varies when the object moves in different speeds. In order to obtain the same length of sequence N in the training step and monitoring step, we normalize the sequence using linear mapping. The impact of linear mapping will be discussed in Subsection IV-B.

The above three sub-procedures are described in Algorithm 1. The input of this algorithm is the raw CP Sequence and the standard power sequence length N. The output is an N-length sequence of CP state $\{-1, 0, 1\}^N$. The "ZeroFilter" function cuts off the abundant runs of "0"s.

Algorithm 1: Data preprocessing

Input: CPSequence;N
Output: CPState
L=length(CPSequence);
for $i = 1 : L$ **do**
  if CPSequence(i) $\uparrow$ **then**
    $temp(i) = 1$;
  end
  else
    if CPSequence(i) $\downarrow$ **then**
      $temp(i) = -1$;
    end
  end
  else
    $temp(i) = 0$;
  end
end
ZeroFilter($temp$);
K=length($temp$);
for $j = 1 : K$ **do**
  CPState($\left[\frac{N-1}{K-1}j + \frac{K-N}{K-1}\right]$) $= temp(j)$;
end

B. Motion profile extraction

As mentioned in Section III, the feature of CP sequence can be uniquely mapped to the trajectory of a moving target. Motion profile extraction intends to answer the follow question: what is the unique feature in a CP sequence that can be used to characterize the motion direction?

As aforementioned in Section III-B, due to the two issues (PBE and IB), we cannot directly match a CP sequence to the trajectory of an object. In order to solve this problem, we repeat this set of experiments by n times and combine the trichotomous sequences of CPs into an $m \times n$ matrix M. Using it as a training data set, we leverage morphological operator to extract a unique motion feature.

In Subsection IV-A, we utilize trichotomous discretization to weaken PBE. However, there are still several PBEs that cannot be eliminated by trichotomy. As a consequence, the CP will be close to the threshold, and a disturbance (*e.g.*, PBE or noise) will force the trichotomous number c flip to another state. Fortunately, this kind of phenomenon neither occurs frequently at the same position, nor lasts during several positions in a row. Therefore, these misclassification errors appear sporadically in matrix M. We can leverage an *opening operator* to handle this situation and erase these isolated noise. Opening operator is a basic morphological mechanism. We briefly illustrate its operating principle. Let E be a Euclidean space or an integer gird, and A be a binary image of E. The erosion of the binary image A by a simple per-defined shape image B is called *structuring element*. It is defined as

$$A \circ B = \bigcup \{B_z \mid B_z \subseteq A\}$$

where B_z is the translation of B by the vector z, *i.e.*, $B_z = \{c \mid c = b + z, b \in B, z \in E\}$. The geometric interpretation of opening operator is to remove all connected components that is fewer than B from a binary image A. In this way, we can eliminate these isolated points from the power matrix. We use $OPENING(A)$ to express opening operation of A by a proper element B. In practice, we leverage the function of opening operator provided by the OpenCV or Matlab library.

In this way, we solve the PBE problem by discretization and the opening operation.

To solve the IB problem, we exploit the dilation, which is another fundamental morphological operator defined as following:

$$A \oplus B = \{z \mid z \in E, (B^s)_z \cap A \neq \varnothing\}$$

where B^s denotes the symmetric of B, *i.e.*, $B^s = \{b \mid -b \in B\}$. The dilation operation probes and expands the shapes contained in the input image A using a structuring element B. The function of dilation operator can also be found in existing scientific computing tools. We use $DILATE(A)$ to express dilating operation of A by a proper element B.

Consider the CP state matrix M, whose element $s_i^j = c$ means the CP of the ith site in the jth experiment is c. Since the dilation has shift invariance, if we dilate two row vectors s^i and s^j, the more overlapping areas we have, the better compatibility between these two vectors can be achieved, or vice versa. Therefore, we propose a metric PEM, *i.e.*, the percentage of nonzero elements in the dilated CP state Matrix M, and use the difference of PEM (DPEM) to detect the most consistence vectors of the CP state vectors. It has three main steps: 1) calculating the PEM of initial CP state matrix M and saving it as PEM; 2) replacing the ith row of M by each test vector in turn, calculating the new PEM of replaced matrix M', and saving it as $Pem(i)$; and 3) calculating the minimum DPEM by $DPEM = ||Pem(i) - PEM||$. We propose Theorem 1 as follows to show that test vectors have no impact on the dilation result of those non-replaced parts. That can also explain that why we can test the PEM row by row.

Theorem 1: if $A = \bigcup A_i$, $A \oplus B = \bigcup (A_i \oplus B)$

Proof:

$$\begin{aligned} A \oplus B &= \{z \mid z \in E, (B^s)_z \cap A \neq \varnothing\} \\ &= \{z \mid z \in E, (B^s)_z \cap (\bigcup A_i) \neq \varnothing\} \\ &= \{z \mid z \in E, \bigcup ((B^s)_z \cap A_i) \neq \varnothing\} \\ &= \bigcup (\{z \mid z \in E, (B^s)_z \cap A_i \neq \varnothing\}) \\ &= \bigcup (A_i \oplus B) \end{aligned}$$

■

Fig. 4 leverages both bars and polar graphs to show the distribution of PEM values for three movement trajectories. It is very clear that PEM values of different movement trajectories are clustered, implying that PEM is a good metric for trajectory classification and recognition.

C. Trajectory recognition

In the training step, we repeat the measurement of the trichotomous sequence S_j^i for each kind of the movement trajectory T_j by N times, and then extract PEM $\mathcal{P}(j)$ for trajectory T_j by performing dilations (see Algorithm 2).

In the monitoring step, we can obtain a trichotomous sequence S_t. In order to identify the actual movement trajectory, we replace each S_j^i with S_t to obtain the motion profile $P(i,j)$, and then calculate the DPEM between $\mathcal{P}(j)$ and $P(i,j)$. For each T_j, we can get a motion profile $DPEM(j) =\mid \mathcal{P}(j) - P(i,j) \mid$. The trajectory T_j with the smallest DPEM is the actual movement trace.

Algorithm 2: Profiling extraction and path identification

Input: S, $testVector$
Output: $path$

$[U, V, N] = size(S)$;
if *in Training Phase* **then**
  for $j = 1 : U$ **do**
    $OPENING(S(j, :, :))$;
    $\mathcal{P}(j) = DILATE(S(j, :, :))$;
  end
end
else
  for $i = 1 : V$ **do**
    $S(:, i, :) = testVector$;
    for $j = 1 : U$ **do**
      $OPENING(S(j, :, :))$;
      $P(i, j) = DILATE(S(j, :, :))$;
    end
  end
  $path = \arg\min_j \{\mid \mathcal{P}(j) - P(i,j) \mid\}$;
end

V. Implementation and Deployment Issues

A. Detection rate and deployment density

In this subsection, we discuss the efficiency of our method compared with the conventional method that is not supporting the direction recognition.

For the ease of presentation, direction recognition can be converted to a problem: how to capture a message over a percolation modeled graph [34]. Suppose a packet K is propagated in an undirected graph $G(V, E)$. In each time period, the packet can move from one vertex V_a to one of its neighboring vertices V_b. During the packet's probing, the vertices that can report whether they receive the packet are called probe vertices, while the rest vertices are defined as the ordinary vertices.

Suppose the percentage of intersections (vertices) that an intruder (packet) passes is s and the deployment density, *i.e.*, the percentage of probe vertices, is α. We present our empirical results on the relationship between α and the detection ratio γ in Fig. 12. We find that if $s > 10\%$, more than 90% of events can be detected with only 20% deployments.

Furthermore, if we deploy EMod at more intersections such that if the $\alpha \to 100\%$, the probability that we can track the complete trajectory of a given packet tends to 1. On the other hand, if the number of "twins" is inadequate, *i.e.*, a small α

that cannot guarantee to capture any given packet in the graph, it is impossible to track the complete trajectory. Therefore, we pursue the optimal setting of α.

There are two conclusions which are useful for solving this problem, guaranteed by percolation theory [34]. Denote the $\theta(\alpha)$ as the probability that we can obtain the whole trajectory of an intruder from the entrance to the exit in graph G, then we have

1) $\theta(\alpha) = 0$ if $\alpha < 1/3$;
2) If G is a 2D square grid, $\alpha = 0.5927$ is the inflection point of θ, *i.e.*, $\frac{d^2\theta}{d\alpha^2}|_{\alpha=0.5927} = 0$.

The above conclusions indicate that, if $\alpha < 1/3$, the intruder is almost impossible to be completely tracked. In other words, if we attempt to identify the entire trajectory of the intruder, the deployment density should not be less than $1/3$.

If α is around 0.5927, the $\theta(\alpha)$ grows most rapidly. In fact, when α is around 0.5927, the growth rate of θ is proportional to $(\alpha - 0.5927)^{-1}$. As a result, more than 80% trajectories can be completely detected when $\alpha \geq 0.7$.

For the motion detection approach with direction recognition, the detection rate (the probability of detecting the moving object at least once) in one intersection is related to the previous intersection whether the motion has been detected, which can be formulated as:

$$Pr\{neighbor(v)_{t+1} = T | v_t = T\}$$

Assume that the percentage of probe vertices is β. For the first movement from the start vertex, the detection rate of K is β, and the missing rate is $1 - \beta$. For each vertex at the trajectory of K, if K in the current vertex is detected with a probability β, it will be detected in the successor vertex with 100% probability. If the previous vertex along the K's trajectory does not detect K, which is with a probability $1-\beta$, its detection rate in the successor vertex is β. The detection rate of K in the vertex along the trajectory is $\beta \times 1 + (1-\beta)\beta = 2\beta - \beta^2$ except for the first vertex, and the missing rate is $1 - (2\beta - \beta^2) = (1-\beta)^2$.

In order to obtain the same detection rate using a motion detection approach without direction recognition, *e.g.*, Twins[16], we set $2\beta - \beta^2 = \alpha$. Then we have $\beta = 0.362$. Compared to the value of $\alpha = 0.7$, we can find that the number of "twins" like detectors required for completely detecting the intruder's trajectory, *i.e.*, the deployment overhead, is cut in half if using EMoD. In other words, EMoD is able to significantly reduce the deployment overhead compared with the non-direction-recognition method.

Note that both Twins and EMoD can be applied to intrusion detection. Twins focuses on checking whether an intrusion occurs in the area of interests, while EMoD can further sketch the intruder's trajectory by leveraging physical layout of the area. As such, EMoD is more suitable for the warehouse or retailing scenarios, which usually contain multiple-row shelves. We detail the performance comparison of these two approach at tracking scenario in Section VI-H.

B. Multipath effects

As aforementioned, most existing device-free approaches utilize the Radio Signal Strength (RSS) variation to detect intruders. In RFID systems, RSS is measured using the received power of RF waves backscattered from a tag. For passive RFID tags, the RSS value varies sharply upon the ambient changes in the backscatter communications, including the disturbance caused by intruders. However, the received wave is the one overlapped by the waves coming from all directions, due to the refection, diffraction, and scattering caused by the furniture, people, and other obstacles. This effect is known as multipath propagation. Upon this effect, the RSS variation cannot accurately reflect the intrusion, because even if there is no any intruder, the RSS value may still change arbitrarily, incurring false alarms or missing reports to the detection result.

EMoD leverages the $critical\ state$ to eliminate the impact from multipath effects. In Twins [16], the authors propose to use the critical state for intrusion detection, which is also utilized by EMoD. Instead of the RSS variation, critical state is able to suppress noise interference. The key insight of critical state can be presented as follows. If two tags are placed within a certain distance, one or both of them become unreadable due to their mutual interference. Keeping the pair of tags in such a state, if an object or human being moves around the tags, some RF waves will be reflected or refracted to the tags, similar to the multipath effect. In this case, the unreadable tag(s) can receive sufficient energy to break the critical state and then become readable, which is called as a state jumping. Clearly, such a "0/1" judgment mechanism will reliably report the motion nearby, avoiding the impact from ambient noises.

C. Real-time requirement

The strict real-time requirement for intruder detection poses another challenge to EMoD. When forcing the tags into critical state for checking whether tags experiences a state shift, a reader should switch the power setting to the predefined CP of each tag. It is very time-consuming for commercial readers to switch their powers among multiple CPs of different tags. For example, switching to a specific power setting takes 0.02s to 0.08s for Impinj reader R220. In the real world, CPs of tags distribute diversely within a wide range, due to the manufacture variation. Note that different locations yield different transmission paths, also leading variant CPs to tags. Hence, it is common that the reader switches its power over a big gap of CPs. As a result, scanning all tags with their CPs will continue several seconds, which can hardly meet the real-time requirement of intrusion detection, considering the intruder may quickly pass the intersections.

EMoD achieves a prompt scanning on the CP samples by adjusting the critical power of tags within a small range. This can be achieved by changing the distance between two tags in a pair of twins [16]. We can probe proper distance between two tags in the twins such that the CPs of all tag pairs (twins) are within a small range, which allows the reader to poll the

scanning on the twins in a very short time duration, *e.g.* merely < 50 ms in our experiments.

Furthermore, we can promote the real-time performance by significantly decreasing the number of tags. According to Slotted ALOHA protocol, which is the mainstream industrial standard for passive RFID tags, the average packet delay

$$\bar{D} = 0.5 + e^G + (e^G - 1)\bar{B} \tag{7}$$

where G is the offered load (packets per unit time) and $\bar{B}$ is the average collision delay, respectively. Since EMoD uses much fewer tags than Twins does, the flux of EMoD is much smaller than that of Twins, *i.e.*, $G_{EMoD} \ll G_{Twins}$. Substituting to (7), $\bar{D}_{EMoD} \ll \bar{D}_{Twins}$, *i.e.*, the packet delay of EMoD is much smaller than that of Twins. In this way, we can promote the real-time performance by decreasing transmitting delay.

D. Particle filter based Realtime Tracking

Once capturing the motion direction at each monitored intersection, it is easy to track the trajectory of the object as time varies. Here we introduce an improved particle filter to track the object. The overview of the algorithm is shown as following:

Initially, the object is located in the intersection (x_0, y_0) where he is detected at the first time. At each time step, the location set is updated based on possible movements and new observations. In our experiments, we assume locations are (x, y) positions in two dimensional Cartesian space.

In the prediction step, we start from the set of possible locations computed in the previous step, L_{t-1}, and apply the mobility model to each sample for getting a set of new samples, L_t. If in previous step l^i_{t-1} is one possible position of an object, the possible current positions are contained in the circular region whose origin is l^i_{t-1} and radius is v_{max}. We use $d(l_1, l_2)$ to denote the Manhattan distance $d(l_{t-1}, l_t) = ||l_{t-1} - l_t||_1$ between two points l_1 and l_2.

$$p(l_t|l_{t-1}) = \begin{cases} \frac{1}{d(l_{t-1}, l_t)} & \text{if } d(l_t, l_{t-1}) < v_{max} \\ 0 & \text{if } d(l_t, l_{t-1}) \geq v_{max} \end{cases} \tag{8}$$

In the cases where the object is detected again at the monitored intersection, the probability distribution can be adjusted for achieving better predictions.

In the filtering step, we filter those impossible locations out based on new observations. We only rely on direct information retrieved from monitored intersections. Let S denote the set of all monitored intersections, r denote the detection range. The filter condition of location l is

$filter(l) = \forall s \in S, d(l, s) < r$

After filtering, the number of possible locations may be smaller than N. In this case, the prediction and filtering processes repeat and union the possible points found, until at least N possible locations can be acquired. After this step, the tracking accuracy will be significantly improved.

Fig. 5. Three experimental environments: Library, Office, and Exhibition hall

VI. Experimental Evaluations

A. Experimental setup

We conduct real experiments in a 28 m $\times$ 15 m indoor area to evaluate the performance of EMoD. We implement EMoD using three types of commodity passive tags, *i.e.*, Impinj E41-b, E41-c, and Alien 964x, a number of commercial passive RFID readers model Impinj SPEEDWAY 220, and off-the-shelf circularly polarized antenna model Laird A9028R30NF. These passive tags have been widely employed in existing logistics and inventory systems. The reader and antenna operate within a spectrum of transmission power from 10 dBm to 32.5 dBm, and a frequency ranging from 920 MHz to 928 MHz. The gain of the antenna is 8 dBi.

The EMoD system operates in three phases, the deploying phase, the learning phase and the monitoring phase. In the deploying phase, we deploy EMoD as shown in Fig. 1. The reader is deployed at one corner of the intersection, *e.g.*, at the point R. Three groups of twins are tightly attached to shelves at other three corners. Hence, slight vibrations will not change the critical power and influence the detection results of EMoD. On the other hand the tags are displaced, *e.g.*, the tags move a short distance due to the shelf displacement, their critical power will change to a new level. However, EMoD identifies the direction of moving objects based on the sequence of tags' critical power changes instead of tags' critical power readings. Thus, the slight displacement of twins will not influence the direction detection.

In the learning phase, we invite 10 volunteers with different genders and body shapes to participate our experiments. Each volunteer moves 10 times from the start point A to each of three destination points, *i.e.*, B, C, and D, to act as turning-left, going-straight, and turning-right, respectively. Volunteers are required to pass through the intersection with normal speed (about 1.5m/s). Therefore, we can obtain the corresponding CP sequences. We set the standard sequence length N as the mode (the most common value among this group) of sequence length and resize other sequences length into N by linear mapping.

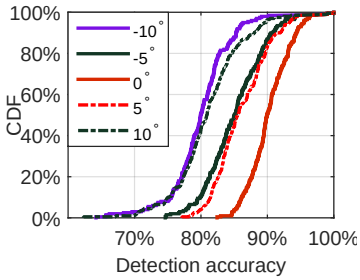

Fig. 6. Impact of angle between reader and tags

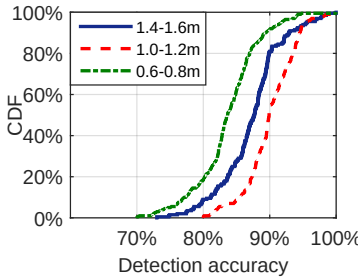

Fig. 7. Impact of tag height

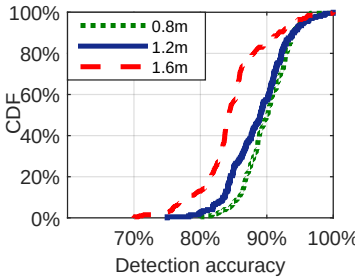

Fig. 8. Impact of intersection width

We extract the j^{th} trajectory profile as $\mathcal{P}(j)$. In the monitoring phase, we resize the length of test CP sequence as N by linear mapping, and calculate the variance of trajectory profile. The trajectory corresponding to the minimum variance of profiles is the actual moving trace.

We verify three typical scenarios for deploying EMoD in real logistic environments, namely the library, office, and exhibition hall, as shown in Fig.5. We examine the overall performance of EMoD in these three scenarios. We also check the performance of EMoD in terms of tag heterogeneity. Finally, we compare the EMoD with Twins [16], which is a most recent device-free motion detection approach using passive tags, to evaluate their detection accuracy.

B. Impact of different angles

The first parameter needed to determine is the deploying angle of the reader's antenna. We use the connecting line between the center of reader's antenna and twins 2 as the baseline. The deploying angle is the horizontal angle between the baseline and the antenna's axis. We then horizontally turn the antenna by $\pm$ 5 degree and $\pm$ 10 degree from the baseline, respectively. Note that if the angle is larger than above setting, *i.e.*, >15 degree or <-15 degree, one tag may be out of the interrogation range of the reader. As shown in Fig. 6, we find that the smaller the angle is, the higher the detection accuracy can be achieved by EMoD. The highest detection accuracy is achieved in the case of 0 degree. In this case, the detection accuracy is nearly 92.5% in average, and 96% for 80% test cases. When the degree of the angle increases, the detection accuracy is degraded. The average detection accuracy is about 87% and 83% for the $\pm$ 5 degree and $\pm$ 10 degree cases, respectively. The feature of reader's beam propagation can explain this phenomenon. The passive RFID reader usually uses the directional antenna, as the one used in our experiment. The pseudo-3D radiation pattern of the reader's main beam propagating in the direction along its antenna's axis is like a spindle. Such a pattern acquires full rotational symmetry along the axis of the directional antenna. If the deploying angle is 0 degree, the twins1 and twins2 will receive approximately equal power density radiated by the antenna. Meanwhile, the two separated areas on both sides of the baseline has a nearly symmetric radiation distribution. These two factors facilitate the two twins functioning equally in the detection, considering their positions are line symmetric to the baseline. If increasing the angle, the asymmetric radiation pattern may degrade the detection effectiveness. Thus, we recommend a 0 degree deploying angle for real implementation.

C. Impact of different heights

We vary the height from 0.8 m to 1.6 m for pursuing the proper height to deploy the twins in EMoD. The results shown in Fig. 7 shows that deploying twins at the height ranging from 1.0 m to 1.2 m yields the highest detection accuracy. When the height is reduced to 0.6 m - 0.8 m, EMoD demonstrates the lowest detection accuracy, nearly 85%. This result implies that different deploying height leads a non-trivial impact to EMoD. From the results, we learn that the discrimination ability of EMoD is nearly maximum when the deploying height is about 1.0 m - 1.2 m. It is interesting to observe that a deploying height within the range of 1.4 m - 1.6 m results in a better performance than that within 0.6 m - 0.8 m. It seems that the ground absorbs RF signals such that the multipath effect becomes weaker near the ground. Based on the result, we adopt a default deploying height as 1.1 m.

D. Impact of moving velocity

We check the effectiveness of EMoD when detecting the object with different moving velocities. It is known that the normal pacing speed of people is about 1.5 m/s. We then conduct the experiments with the default settings proposed in previous subsections, while using two velocity settings, namely *normal* (1.5 m/s) and *high* (3 m/s). Each volunteer walks through the intersection 10 times for each velocity.

Fig. 10 depicts the detection accuracy of EMoD upon the two velocities. The results show that the normal moving velocity enables a detection accuracy of 93.3%+, while the accuracy of high moving velocity is around 91%. As the normal moving speed is used in the training stage, the number of sampling points in monitoring stage is similar with the training data, and the detection performance is relatively better. High moving speed causes the sub-sampling problem, which will affect the CP distribution matching. Fortunately, we introduce PEM to represent the trajectory profile, which can adaptively adjust the coefficient of expansion according to the number of sampling points. With an increase of moving speed, the coefficient of expansion will increase and the PEM may keep relatively stable for the same trajectory.

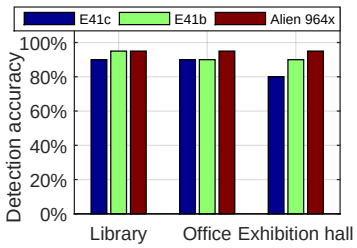

Fig. 9. Impact of different tags

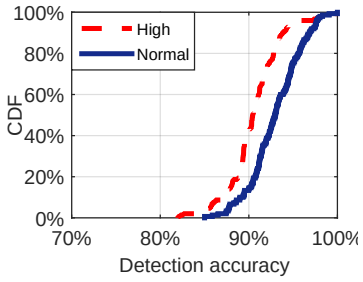

Fig. 10. Impact of different velocities

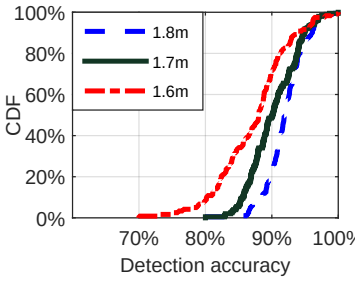

Fig. 11. Impact of different people

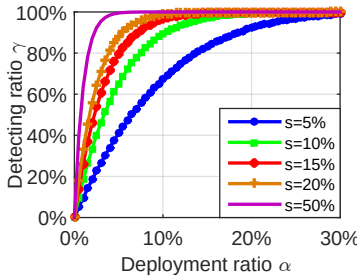

Fig. 12. Relationship between detection ratio and deployment ratio

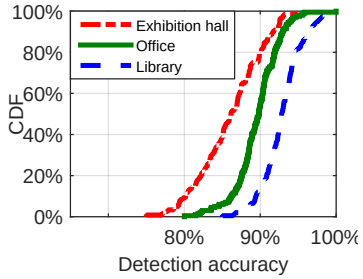

Fig. 13. Overall performance

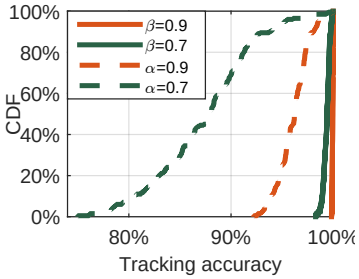

Fig. 14. Tracking accuracy comparison

E. Impact of object height

The volunteers involved in our experiments can be categorized into three group by their heights, *i.e.*, around 1.6 m, 1.7 m, and 1.8 m. We investigate the detection accuracy in above heights. The results plotted in Fig. 11 imply that the height of moving object has a certain impact on the detection accuracy. The taller the volunteer is, the higher the detection accuracy EMoD can achieve. In particular, the accuracy of detecting the group of volunteers with the height of 1.8 m is 93% in average. As analyzed in [16], a taller person contributes a larger area that reflects (or blocks) more RF signals to the twins. In short, the influence to the twins will be augmented if a taller person moves into the monitoring area. In this way, the three twins have more opportunities to generate distinct features corresponding to the specific direction. However, the accuracy of detecting those volunteers with the height around 1.6 m is 87% in average, indicating that EMoD is still effective in the direction prediction.

F. Impact of variant scenarios

We simulate three typical scenarios, library, office, and exhibition hall, by varying the width of the aisles. We choose their settings of width as 0.8 m, 1.6 m, and 3.2 m, respectively. We find that if the width is set to 0.8 m, the detection accuracy can reach 95%. The setting of 1.6 m was relatively a little worse. In the case of 3.2 m, the accuracy declines obviously. The results show that the width of the aisles can influence the discrimination ability of EMoD on the moving object's direction. In a narrow aisles, the possible area that a person moves is limited. Thus, the output of PEM has a small variance, indicating a high detection accuracy. On the contrary, a wide aisles gives more space to the person passing through. The output of PEM suffers from a large variance, resulting in a lower detection accuracy. In practice, we suggest the width of aisles is not larger than 3.2 m, which can provide an 87%+ detection accuracy in average.

G. Impact of tag heterogeneity

In above experiment, we mainly use the Impinj E41-c (E41-c for short). We then repeat the experiments by replacing the passive tag with Impinj E41-b (E41-b for short) and Alien 964x, with the same experiment settings. Fig. 9 plots the performance when leveraging different types of tags in EMoD. We find that the E41c tag produces the best performance, with a detection accuracy as 91%. The detection accuracy when using Alien 964x or E41-b tags is relatively lower. But the lowest one is still 86%+. Such a result demonstrates that EMoD is resilient to the tag heterogeneity.

H. Comparison with Twins

Twins [16] is the latest work for device-free localization and tracking using passive RFID tags. We perform a large scale simulation to evaluate the tracking accuracy between EMoD and Twins with different coverage. In our simulation, there are 50 intersections. Fig. 14 compares the tracking accuracy between Twins and EMoD. The α and β denotes the coverage of Twins and EMoD in intersections, respectively. The tracking accuracy is that the ratio of correct estimated trajectory with real trajectory. Twins can only detect the object without moving direction, so it can not estimate the location of object in un-monitoring intersection. It fails to tell us where the object has come from and where he is going to.

If the coverage area shrinks, the tracking accuracy of Twins decreases sharply. When α is 70%, the tracking accuracy drops to 87%. In contrast, with the increase of β, the tracking accuracy of EMoD increases significantly. When β is 70%, the tracking accuracy is higher than 98%. It is because that an accurate detection can exactly estimate the trajectories in previous intersection and next intersection. In other words, EMoD can forecast the location of object in next intersection and infer the orientation of object in prior intersection, once an intruder is detected in current intersection.

VII. Conclusion and Future Work

In this paper, we propose a novel method to detect the motion of device-free objects using sparsely deployed passive RFID tags. Our solution, namely EMoD, can effectively detect and track the device-free intruders only with a few of pairs of passive tags deployed in critical points. In particular, we design a real-time direction indication algorithm to facilitate efficient motion detection. We theoretically analyze the feasibility of EMoD and conduct extensive experiments for performance evaluation. The results show that EMoD overcomes the drawbacks of dense or full-coverage deployment and infeasibility of direction prediction, while achieving high accuracy in device-free motion detection. Our future work includes extending the implementation of EMoD to 3D scenario, further improving the detection accuracy, and introducing the direction prediction algorithm of EMoD to other RF based systems.

VIII. Acknowledgement

We would like to thank our shepherd Fahad R. Dogar, and the anonymous reviewers, for their useful comments. This work is supported by NSFC Grant 61190112, 61325013, 61373175, 61402359, and China 863 Grant 2013AA014601. Chen Qian is supported by University of Kentucky College of Engineering Faculty Startup Grant and National Science Foundation grant CNS-1464335.

References

[1] L. M. Ni, Y. Liu, Y. C. Lau, and A. P. Patil, "LANDMARC: indoor location sensing using active RFID," *Wireless networks*, vol. 10, no. 6, pp. 701–710, 2004.

[2] Y. Zhao, Y. Liu, and L. M. Ni, "VIRE: Active RFID-based localization using virtual reference elimination," in *IEEE ICPP'2007*.

[3] D. Zhang, J. Zhou, M. Guo, J. Cao, and T. Li, "TASA: Tag-free activity sensing using RFID tag arrays," *IEEE TPDS*, vol. 22, no. 4, pp. 558–570, 2011.

[4] Wang, Jue and Vasisht, Deepak and Katabi, Dina, "RF-IDraw: virtual touch screen in the air using RF signals," in *ACM SIGCOMM'2014*.

[5] J. Wang and D. Katabi, "Dude, where's my card? RFID positioning that works with multipath and non-line of sight," in *ACM SIGCOMM'2013*.

[6] J. Wang, F. Adib, R. Knepper, D. Katabi, and D. Rus, "RF-compass: robot object manipulation using RFIDs," in *ACM MobiCom'2013*.

[7] F. Adib and D. Katabi, "See through walls with WiFi!" in *ACM SIGCOMM'2013*.

[8] F. Adib, Z. Kabelac, D. Katabi, and R. C. Miller, "3D tracking via body radio reflections," in *NSDI'2014*.

[9] Q. Pu, S. Gupta, S. Gollakota, and S. Patel, "Whole-home gesture recognition using wireless signals," in *ACM MobiCom'2013*.

[10] Kellogg Bryce, Talla Vamsi, and Gollakota Shyamnath, "Bringing gesture recognition to all devices," in *Usenix NSDI'2014*.

[11] Adib, Fadel and Kabelac, Zachary and Katabi, Dina, "Multi-person localization via RF body reflections," in *NSDI'2015*.

[12] Qian, Chen and Liu, Yunhuai and Ngan, Hoilun and Ni, Lionel M, "Asap: Scalable identification and counting for contactless rfid systems," in *IEEE ICDCS'2010*.

[13] Qian, Chen and Liu, Yunhuai and Ngan, Raymond Hoilun and Ni, Lionel M, "ASAP: Scalable collision arbitration for large RFID systems," *IEEE TPDS*, vol. 24, no. 7, pp. 1277–1288, 2013.

[14] Xi, Wei and Zhao, Jizhong and Li, Xiang-Yang and Zhao, Kun and Tang, Shaojie and Liu, Xue and Jiang, Zhiping, "Electronic frog eye: Counting crowd using WiFi," in *IEEE INFOCOM'2014*.

[15] Yang Lei, Chen Yekui, Li Xiang-Yang, Xiao Chaowei, Li Mo and Liu Yunhao, "Tagoram: real-time tracking of mobile RFID tags to high precision using COTS devices," in *ACM MobiCom'2014*.

[16] H. Jinsong, Q. Chen, M. Dan, W. Xing, Z. Jizhong, Z. Pengfeng, X. Wei, and J. Zhiping, "Twins: Device-free object tracking using passive tags," in *IEEE INFOCOM'2014*.

[17] J. S. Choi, H. Lee, D. W. Engels, and R. Elmasri, "Passive UHF RFID-based localization using detection of tag interference on smart shelf," *IEEE TSMC*, vol. 42, no. 2, pp. 268–275, 2012.

[18] T. Liu, L. Yang, Q. Lin, Y. Guo, and Y. Liu, "Anchor-free backscatter positioning for RFID tags with high accuracy," in *IEEE INFOCOM'2014*.

[19] K. Bu, X. Liu, J. Li, and B. Xiao, "Less is more: Efficient RFID-based 3D localization," in *IEEE MASS'2013*.

[20] M. Youssef, M. Mah, and A. Agrawala, "Challenges: device-free passive localization for wireless environments," in *ACM MobiCom'2007*.

[21] C. Liu, D. Fang, Z. Yang, X. Chen, W. Wang, T. Xing, N. An, and L. Cai, "RDL: A novel approach for passive object localization in WSN based on RSSI," in *IEEE ICC'2012*.

[22] X. Zheng, J. Yang, Y. Chen, and Y. Gan, "Adaptive device-free passive localization coping with dynamic target speed," in *IEEE INFOCOM'2013*.

[23] J. Wang, D. Fang, X. Chen, Z. Yang, T. Xing, and L. Cai, "LCS: Compressive sensing based device-free localization for multiple targets in sensor networks," in *IEEE INFOCOM'2013*.

[24] Y. Liu, Y. Zhao, L. Chen, J. Pei, and J. Han, "Mining frequent trajectory patterns for activity monitoring using radio frequency tag arrays," *IEEE TPDS*, vol. 23, no. 11, pp. 2138–2149, 2012.

[25] S. Guha, K. Plarre, D. Lissner, S. Mitra, B. Krishna, P. Dutta, and S. Kumar, "Autowitness: locating and tracking stolen property while tolerating GPS and radio outages," *ACM TOSN*, vol. 8, no. 4, p. 31, 2012.

[26] C. Xu, B. Firner, Y. Zhang, R. Howard, J. Li, and X. Lin, "Improving RF-based device-free passive localization in cluttered indoor environments through probabilistic classification methods," in *ACM IPSN'2012*.

[27] C. Xu, B. Firner, R. S. Moore, Y. Zhang, W. Trappe, R. Howard, F. Zhang, and N. An, "SCPL: indoor device-free multi-subject counting and localization using radio signal strength," in *ACM IPSN'2013*.

[28] S. Tang, X.-Y. Li, H. Zhang, J. Han, G. Dai, C. Wang, and X. Shen, "TELOSCAM: Identifying burglar through networked sensor-camera mates with privacy protection," in *IEEE RTSS'2011*.

[29] Z. Zhou, Z. Yang, C. Wu, L. Shangguan, and Y. Liu, "Towards omnidirectional passive human detection," in *IEEE INFOCOM'2013*.

[30] J. Xiao, K. Wu, Y. Yi, L. Wang, and L. M. Ni, "Pilot: Passive device-free indoor localization using channel state information," in *IEEE ICDCS'2013*.

[31] W. Xi, J. Zhao, X.-Y. Li, K. Zhao, S. Tang, X. Liu, and Z. Jiang, "Electronic frog eye: Counting crowd using WiFi," in *IEEE INFOCOM'2014*.

[32] G. Franceschetti and S. Stornelli, *Wireless Networks: From the Physical Layer to Communication, Computing, Sensing and Control*. Academic Press, 2006.

[33] R. Serway and J. Jewett, *Physics for scientists and engineers*. Cengage Learning, 2013.

[34] D. Stauffer and A. Aharony, *Introduction to percolation theory*. Taylor and Francis, 1994.

[35] M. K. Pitt and N. Shephard, "Filtering via simulation: Auxiliary particle filters," *Journal of the American statistical association*, vol. 94, no. 446, pp. 590–599, 1999.